

# PCL micro-dumbbells – A new class of polymeric particles reveals morphological biofunctionality

David Sonnleitner<sup>a</sup>, Natascha Schäfer<sup>b</sup>, Annalena Wieland<sup>c</sup>, Lena Fischer<sup>d</sup>,  
Patrick Pasberg<sup>a</sup>, Ingo Thievensen<sup>d</sup>, Gregor Lang<sup>a,\*</sup>

<sup>a</sup> Biopolymer Processing, Faculty of Engineering Science, University of Bayreuth, Ludwig-Thoma-Str. 36a, 95447 Bayreuth, Germany

<sup>b</sup> Institute of Clinical Neurobiology, University Hospital, Julius-Maximilians-University of Würzburg, Versbacherstr. 5, 97078, Würzburg, Germany

<sup>c</sup> Department of Gynecology and Obstetrics, Laboratory for Molecular Medicine, University Hospital Erlangen, Friedrich-Alexander-University (FAU) Erlangen-Nuernberg, Universitätsstrasse 21-23, 91054 Erlangen, Germany

<sup>d</sup> Biophysics Group, Department of Physics, Friedrich-Alexander-University of Erlangen-Nuremberg, Henkestr. 91, 91052 Erlangen, Germany

## ARTICLE INFO

### Article history:

Received 24 March 2021

Revised 26 May 2021

Accepted 11 June 2021

### Keywords:

Tissue engineering

Fibers

Particles

Electrospinning

Polycaprolactone

## ABSTRACT

Biopolymeric particles can be fibrous or spherical, highly determining their areas of medical applications such as biomimetic fibers for tissue engineering or injectable capsules. In this work, we present a completely novel morphology, combining structural features of fibers and spheres in dumbbell-shaped Poly- $\epsilon$ -Caprolactone (PCL) micro-particles. Strikingly, such complex structures could be achieved by simply balancing out the parameters of a standard electrospinning setup together with fine-tuned spinning dope compositions. In-situ entropy-elastic snapping of deposited fibers could be triggered by combining PCL with different molecular weights, allowing for control over the aspect ratio of generated dumbbells in an accurate manner. With a single electrospinning nozzle, high production rates in the range of 80.000 dumbbells per second were achieved. To assess morphologically induced biofunctionality, dumbbell suspending and surface modification with collagen was performed and in vitro-testing with U87 reporter cells demonstrated significantly enhanced integrin-based cell adhesion on PCL-dumbbells as compared to continuous PCL-fibers. The results clearly unravel the remarkable potential of such structures in the field of tissue engineering. Revealing this new class of polymeric particles will also open the door to various new approaches including injectables, biofabrication and cosmetics, moreover, defining a novel type of filler material.

© 2021 The Authors. Published by Elsevier Ltd.

This is an open access article under the CC BY license (<http://creativecommons.org/licenses/by/4.0/>)

## 1. Introduction

Among the synthetic materials suitable for biomedical applications, Poly- $\epsilon$ -Caprolactone (PCL) has gained outstanding interest within the last decades. The semi-crystalline linear aliphatic polyester is biocompatible and biodegradable, belonging to the class of synthetic biopolymers [1]. It was first synthesized in the 1930s [2] but did not receive significant attention until the demand on resorbable polymers arose at the end of the 20th century. PCL can be degraded via surface or bulk hydrolytic pathways rendering it a biodegradable material [3]. Furthermore, its thermal properties of low glass transition ( $-60$  °C) and melting temperature ( $60$  °C), resulting in straightforward processing, as well as relatively

inexpensive production routes promoted its prevalence in science and industry [4]. Finally, commercial break through was induced by FDA-approval (U.S. Food and Drug Administration) of biomedical PCL-based products like Monocryl® [5]. With the subsequent CE certification, various other applications such as wound dressings, contraceptive devices, implants for tendon repair or dentistry have opened up within the last two decades [6–9]. This success story is ongoing, and the number of annually published articles referring PCL is constantly increasing (more than 2000 publications in 2019), with explicitly growing focus on work with electrospun PCL-fibers in various compositions ( $\sim 350$  in 2019) [10].

In general, PCL can be processed into a broad variety of morphologies, from films to spheres and foams as well as 3D-scaffolds, which are produced by selective laser sintering or fused deposition modeling [11–15]. Furthermore, electrospinning in general provides a highly attractive, fast and relatively simple method to generate fibers with diameters in the micro-, submicro-, and

\* Corresponding author.

E-mail address: [Gregor.Lang@uni-bayreuth.de](mailto:Gregor.Lang@uni-bayreuth.de) (G. Lang).

nanoscale [16,17]. Thereby, a polymer solution or melt is extruded from a needle, which is connected to a high voltage source (up to 100 kV) inducing electrostatic surface charges at the droplet's interface [18]. Coulombic repulsion in the spinning dope leads to formation of a Taylor cone with jet ejection as the surface tension is overcome by the electrostatic forces. The jet is stretched due to acceleration and whipping and simultaneously solidifies as a result of drying or cooling [19]. The resulting fibers are attracted by a counter-charged or grounded collector, which can be a simple plate to create nonwovens, or e.g., rotating drums for aligned fibers [20,21]. The broad magnitude of fiber diameters and variety of material compositions, that can be fabricated via electrospinning, has aroused significant interest in the fields of tissue engineering (TE) and regenerative medicine (RM). Thereby, the main focus is on mimicking the morphological features of the natural extracellular matrix (ECM) to provide cell-friendly environments by design [22]. ECM is a tissue specific and non-cellular component present within all tissues and organs. It provides physical scaffolding for cells, but also crucial biochemical and biomechanical cues that are required for cell or tissue morphogenesis, differentiation and homeostasis [23]. The main groups of fibrous ECM proteins are collagens, elastins, fibronectins and laminins [24]. Cell adhesion to the ECM is mediated by ECM receptors on the cellular surface such as for example integrins [25]. Interaction or adhesion of cells with their integrins further leads to cytoskeletal coupling to the ECM and is therefore involved in cell migration and adhesion on and through the ECM [26]. Both processes depend on organization of the actin cytoskeleton (F-Actin) into adhesive and protrusive organelles in response to extracellular signals [27]. Numerous studies applying different cell types have shown the positive impact of mimicking ECM-like fibrillar structures via electrospinning. Wise et al. demonstrated that human mesenchymal stem cells, seeded on aligned electrospun PCL fibers ( $\varnothing$  500 nm and 3  $\mu$ m), adapted to axial orientation resulting in enhanced chondrogenic differentiation on 500 nm fiber scaffolds as compared to 3  $\mu$ m fibers and the control without fibers [28]. In another study, the penetration depth of human venous myofibroblasts into different electrospun nonwovens ( $\varnothing$  3–12  $\mu$ m) was investigated and it was found that the largest diameter ( $\varnothing$  12  $\mu$ m) provided optimal, unobstructed cell infiltration [29]. This emphasizes the variability in structure-specific cell response and the need for application-related optimization of material morphologies. Another important aspect of such fibers is their biological surface functionality. As presented by Schnell et al., a blend of 75:25 wt% of PCL and collagen as spinning dope, significantly improved Schwann cell migration, neurite orientation and filopodial extension of Schwann cells and fibroblasts in comparison to pure PCL fibers [30]. Comparable effects were further demonstrated by Krithica et al., who presented a strategy to immobilize type I collagen on PCL nanofibers that enhanced fibroblast attachment and growth on the coated fibers [31].

Besides electrospun non-woven meshes or aligned fiber mats, that often result in 2D substrates, short fibers were recently identified as highly attractive morphology to render electrospun fibers accessible for applications such as supplements for injectables, bioinks in biofabrication or as a replacement for microcapsules in cosmetic products [32–34]. Regarding PCL, the main focus so far was on the production of continuous electrospun fibers and electrospayed microspheres with diameters ranging from 0.5–5  $\mu$ m for fibers and 1–50  $\mu$ m for microspheres [35–37]. To produce the attractive morphology of short fibers, most approaches require consecutive fragmentation steps (UV-irradiation or hydrolyses) after the production of a sufficient number of continuous fibers. By contrast, self-formation of fragmented fibers during electrospinning was previously observed, but not further investigated as it was undesired and interpreted as large beads [38].

Addressing the growing demand on such advanced polymer morphologies, we established a simple electrospinning approach to in-situ fabricate dumbbell-shaped PCL fiber fragments by precisely balancing out processing conditions. We could demonstrate, that applying a well-defined parameter set in a standard electrospinning device with a mesh substrate (Fig. 1A) resulted in fiber snapping and thus fragment formation in a onestep process (Fig. 1B). Hypothesizing, that this phenomenon is intrinsically driven by entropy elastic forces of PCL molecules, we were able to transfer our findings and adjust fiber length by blending PCL of different molecular weight (MW). Finally, we assessed, that the combination of structural features of spheres and fibers within this new micro-particle system might induce morphologically triggered, biologically relevant features. Therefore, we performed reporter cell culture experiments on collagen-modified PCL (Fig. 1C) displaying significant impact of our dumbbell morphology on cell performance as compared to continuous fibers. Remarkably promoted cell adhesion and spreading was attributed explicitly to integrin-based cell adhesion at the curvature of collagen-coated PCL-dumbbells.

## 2. Materials and methods

### 2.1. Electrospinning

Polycaprolactone with three different molecular weights (10/45/80 kDa, Sigma-Aldrich, MO, USA) was dissolved overnight at room temperature in 99% pure 1,1,1,3,3,3-hexafluoro-2-propanol (HFIP, abcr GmbH, Germany) to form 20%w/v and 30%w/v solutions. The solutions were loaded into 3 ml syringes (Omnifix® Luer Lock Solo, B. Braun, Germany) and placed in the syringe pump (KDS 200, KD Scientific Inc., MA, USA) with the volume flow set to 1 ml/h. The syringes were connected to stainless-steel needles (21 G, Cat. No.371.0820, Socorex Isba SA, Switzerland) through luer-lock connecting tubes (B.Braun Perfusor line 30 cm) to reach the inside of the spinning chamber. A custom-made rotating drum ( $\varnothing$  85 mm) was set-up with a constant rotating speed of 100 RPM for random non-woven and 10 000 RPM for aligned fibers. The rotating drum was covered with collecting mesh made of polyester (Mesh size 80  $\mu$ m, Reichelt Chemietechnik GmbH+Co, Germany.) as collecting substrate. The distance between the tip of the needle and the collecting drum was fixed to 9 cm and high voltage was applied at the needle (+4 to +6 kV) and the collector (–1 kV). Samples for morphological analysis were spun for 20 min, samples for cell culture experiments for 60 min to reach sufficient layer height.

### 2.2. Fiber fragment disassembly

The generated coated carrier meshes were removed from the drum and immersed in ethanol. After 20 min, the nonwoven could be easily peeled off, cut into smaller pieces and subjected to ultrasonication to suspend the individual fragments from the bulk material. Ultrasonication was applied for about two hours using flat probe ultrasonic processor (UP200Ht, flat probe diameter 40 mm, Hielscher Ultrasonics GmbH, Germany) at 70% amplitude and pulse duration of 2:1 (On:Off), sonication power was adjusted automatically based on amplitude and pulse setting. During sonication, the PCL sheets were suspended in ethanol and cooled below 10 °C to prevent melting of PCL. The PCL fiber fragments were filtered twice using coarse filters (Mesh size 105  $\mu$ m, Reichelt Chemietechnik GmbH+Co., Germany) and fine filters (Mesh size 45  $\mu$ m, Reichelt Chemietechnik GmbH + Co., Germany). The turbid filtrate

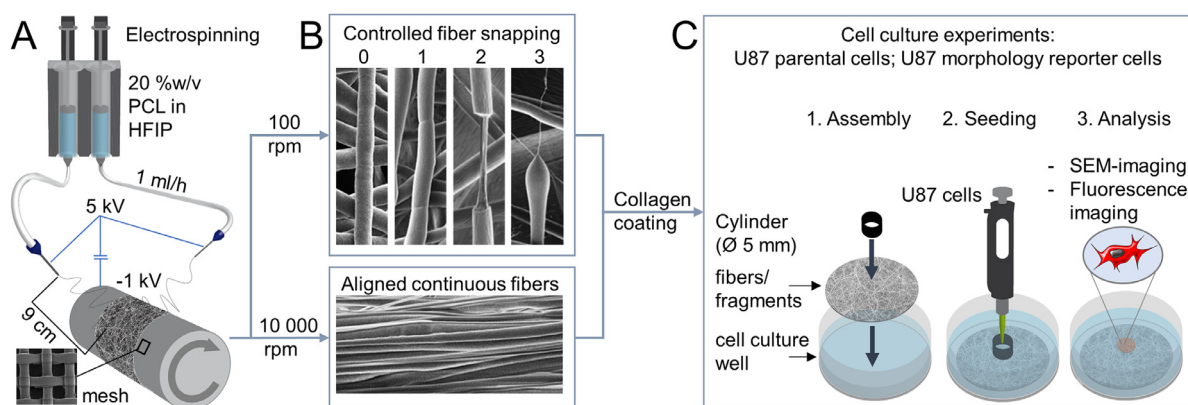


**Fig. 1.** Schematic overview on the presented approach: (A) Parameter set of a standard electrospinning device with a mesh substrate was specified to induce fiber snapping (controlled by MW composition of PCL-blends) resulting in dumbbell-like structures (B). These structures were biofunctionalized with a collagen coating and tested in-vitro with U87 reporter cells (C).

was dried at 37° for 7 days until a dry pellet was formed that allowed easy storage and full resuspension.

### 2.3. Collagen coating

Samples for coating were immersed in 10% 1,6-hexanediamine (Sigma Aldrich, MO, USA) in 2-propanol and mixed in an overhead stirrer at RT for 1 h. The samples were washed thoroughly with an excess of Milli-Q water several times and lyophilized afterwards for 12 h. The dry samples were immersed in 1% glutaraldehyde for 1 h at room temperature. The samples were washed several times with Milli-Q water and suspended in 2.5 mg ml<sup>-1</sup> collagen solution (ibidi GmbH, Germany) at pH 3.4 and gently mixed at 2–4 °C for 48 h. Samples were filtered and rinsed once with 0.1% acetic acid and subsequently with Milli-Q water until neutral pH was reached. The samples were dried under the fume hood at RT overnight prior to the experiments. 24-Well plates for life-imaging with zenCELL owl were coated as follows: 250 µl collagen solution (Corning Cat. No.: 354,249; 9,88 mg/mL) were diluted in 15 mL 20 mM acetic acid. 250 µl were added to each 24-well and kept for 1 h at RT. Afterwards collagen was removed and wells were washed 3x with PBS.

### 2.4. Scanning electron microscopy (SEM), energy dispersive X-ray analysis (EDX) and X-ray photoelectron spectroscopy (XPS)

The samples were cut from the supporting mesh and placed on SEM stubs. Resuspended and coated fiber fragments were pipetted on round glass slides and dried overnight under the fume hood. All samples were sputtered (EM ACE600, Leica Microsystems, Germany) with a 2 nm layer of platinum prior to analysis. Scanning electron microscopy (Apreo Volumescape, FEI/ThermoScientific, MA, USA) was used to analyze the morphology of the electrospun fiber fragments as spun and after the coating procedures. High vacuum was applied with the Everhart-Thornley-Detector operating in standard mode with an accelerating voltage of 2 kV and a working distance of 10 mm. ImageJ (National Institutes of Health, MD, USA) was used to determine the fiber diameters from SEM micrographs with at least 100 measured features per sample. Energy Dispersive X-ray analysis (EDX) and X-ray Photoelectron Spectroscopy (XPS) were used to detect introduced nitrogen groups on the surface of the fragments during the coating procedure. EDX was used in low vacuum mode with an acceleration voltage of 1.0 kV. XPS was performed with a VersaProbe III Scanning XPS Microprobe (Physical Electronics GmbH, Germany) using the monochromatised Al K-alpha beam with 100 µm beam size.

### 2.5. Fourier-transform infrared spectroscopy

Dry samples of coated and uncoated fiber fragments were investigated with a FT-IR spectrometer (InfraRed Bruker Tensor 37, Bruker Corporation, MA, USA) using the ATR Ge-crystal setup in direct contact mode. All spectra were measured in absorbance mode with atmospheric compensation enabled with a resolution of 4 cm<sup>-1</sup> and a sample scan time of 100 scans in the range from 4000 to 800 cm<sup>-1</sup>. A background scan was performed prior to the samples and subsequently subtracted from all spectra. One step baseline correction was applied during data evaluation for better comparability.

### 2.6. Contact angle

Contact angle measurement (Surftens universal, OEG GmbH, Germany) was used to assess the surface wettability of the coated and uncoated samples. Every measurement was repeated 5 times with a droplet volume of 0.5 µl Milli-Q H<sub>2</sub>O.

### 2.7. Reporter cell generation

For the generation of lentiviral transfer vector, cDNA of farnesylated tdTomato fluorescent protein was amplified from tdTomato-farnesyl-5 plasmid (Addgene, #58,092) using a 5' primer encoding a BamHI site and a 3' primer encoding a NotI site, and used to replace the AcGFP cDNA in pLVX-AcGFP-N1 (Clontech, #632,154). Following purification of the PCR product, it was treated with BamHI and NotI and inserted into the similarly treated vector pLVX-AcGFP-N1. After purification of the plasmid DNA using the NucleoBond Xtra Maxi Kit (Macherey-Nagel, #740,414.50) its sequence was verified by custom DNA sequencing (Eurofins Genomics Germany GmbH, Germany). Lentivirus was generated by co-transfecting the transfer plasmid with the packaging plasmid psPAX.2 (Addgene, #8454) and the enveloping plasmid VSV-G (Addgene, #12,260) in LentiX 293 T cells (Takara, # 632,180) using Lipofectamine 2000 (ThermoFisher Scientific, #11,668,019). The virus-containing supernatant was harvested after 48 h of incubation and briefly centrifuged. Using the LentiX concentrator (Takara, #631,232), lentivirus was concentrated (10 x) and then used for reverse transduction of U87 cells (U-87 MG, ATCC® HTB-14™, LGC Standards GmbH, Germany). The infection was carried out by seeding U87 cells at a density of 100,000 per 9.6 cm<sup>2</sup> on top of previously dispensed lentivirus. U87 cells, stably expressing the reporter construct were further selected with puromycin (3 µg ml<sup>-1</sup>) to obtain U87 non-clonal cell lines.

## 2.8. Cell culture

U87 cells and TdTomato-farnesyl expressing U87 reporter cells were cultured in Minimal Essential Medium (MEM) (21,090–055, Gibco, MA, USA) supplemented with 10% FCS (10,270–106 Life Technologies, MA, USA), 1% Penicillin 50 U ml<sup>-1</sup>, Streptomycin 50 µg ml<sup>-1</sup> (15,140–122 Life Technologies, MA, USA), 1% 200 mM GlutaMAX (35,050–038 Life Technologies, MA, USA), 1% 100 mM sodium pyruvate (11,360–039 Life Technologies, MA, USA). Cells were seeded in a density of 20,000 cells into the inner part of a hollow cylinder (polytetrafluoroethylene) with an outer diameter of 8.6 mm, inner diameter of 5 mm and a height of 10 mm placed upon electrospun samples. Samples were incubated for 2 h at 37 °C and 5% CO<sub>2</sub> prior to removal of the hollow cylinder. Cells were kept at 37 °C and 5% CO<sub>2</sub> for 96 h following immunocytochemical staining.

## 2.9. Life/dead assay

Cells were grown on electrospun samples for 24 h in a density of 30,000 cells. Samples were incubated for 30 min at 21 °C with  $2 \times 10^{-6}$  M calcein AM (green/living cells; Thermo Fisher Scientific, MA, USA) and  $2 \times 10^{-6}$  M ethidium homodimer I (red/dead cells, Sigma-Aldrich, MO, USA) in 1x PBS. Right after incubation cells were imaged.

## 2.10. Immunocytochemistry

Cells were washed with 1x PBS, fixed with 4% PFA/Sucrose for 15 min, following blocking with 5% normal goat serum and 0.1% Triton-X100 for 30 min. Cells were incubated with ActinGreen™ 488 ReadyProbes™ Reagent (AlexaFluor™ 488 phalloidin, R37110, Invitrogen Thermo Fisher Scientific, MA, USA, dilution 1:50 in 5% NGS) for 1 h. After three washing steps cells were mounted with Mowiol.

## 2.11. Live cell imaging

U87 cells were seeded on collagen coated vs non-coated 24-wells in a density of 30,000 cells. The media was enriched with and without free floating fibers in a density of 1 mg/ml. After 2 h 24-well plate were placed into a zenCELL owl life cell imaging microscope (InnoME GmbH, Germany) for 3 days. Wells were recorded every 17 min and cell coverage, number of adherent cells, number of non-adherent cells and total number of cells for each single culture well was monitored. Diagrams and videos of life cell imaging were acquired using zenCELL owl software version 3.3.

## 2.12. Confocal microscopy and image processing

Images of immunocytochemical stainings were acquired using an inverted Olympus iX81 microscope (Olympus Corporation, Japan) equipped with diode lasers of 405 nm (DAPI), 473 nm (Alexa488), 559 nm (Cy3). All images shown were acquired using an Olympus UPLSAPO 60x (oil, numerical aperture: 1.35) objective. Images of Life/dead assay were taken using an inverted microscope (Olympus IX83, cellSens Software V1.16, Olympus Corporation, Japan). ImageJ-software (National Institutes of Health, MD, USA) was used for further image processing and counting of cells numbers [39].

## 3. Results and discussion

### 3.1. Fabrication of dumbbell shaped microfiber fragments by electrospinning

In this work, we identified a new phenomenon leading to fragmentation of PCL fibers upon electrospinning. Initially, the ideal

electrospinning parameters that allow for reproducible fiber snapping were experimentally determined (Fig. 1A). Via SEM analysis of electrospun PCL (45 kDa, 20%w/v in HFIP) we could classify four different stages (Fig. 1B) showing deposited fibers (0), necking (1), contraction (2) and snapping (3). We hypothesize, that as soon as the fiber is deposited and the extensional forces within the electric field are gone, entropy elastic effects take over. In other work, it was shown that electrospinning conditions, irrespective to molecular weight, solvent systems and concentration, have no significant impact on the degree of crystallinity of PCL [40]. Nevertheless, it is hypothesized that two competing effects take place upon electrospinning. On the one hand, the fast evaporation of the solvent might result in reduced crystallinity as crystal nucleation kinetically needs time. On the other hand, there is a pronounced stretching of the polymer solution, especially in the whipping region leading to a high degree of molecular orientation. The latter promotes crystallization resulting in anisotropic semi-crystalline structures [41]. Molecular relaxation of this anisotropy resulting in the build-up of internal stress was supposed to be the origin of fiber snapping. To test our hypothesis, the impact of MW on fiber morphology was analyzed via SEM-imaging (Fig. 2). It could be shown that MW plays a crucial role in the fragmentation behavior as the length of the polymer chains determines the degree of molecular entanglement. Short chains (10 kDa) resulted in electrospinning (Fig. 2A), as shown in the previous literature [42], producing spheres with a diameter of  $11.1 \pm 3.1$  µm. In medium MW PCL (45 kDa), the chains were long enough to form a stable jet but could not withstand the subsequent entropy elastic stress resulting in fiber fragments with a length of  $54.9 \pm 28.7$  µm and a diameter of  $2.5 \pm 0.6$  µm, thus displaying an aspect ratio of  $22.5 \pm 11.8$  (Fig. 2B). Increased molecular entanglement in high MW PCL (80 kDa) on the other hand resulted in continuous fibers with a diameter of  $2.4 \pm 0.3$  µm (Fig. 2C). Furthermore, we could clearly verify, that snapping happens after deposition of the fibers on the collector (Fig. S1) and could be promoted by electrospinning free-hanging fibers bridging the gaps of a micro-mesh substrate as shown in Fig. 2.

Strikingly, based on our findings and the theory of entropy elastically driven contraction, we were able to induce fiber snapping by blending high MW with low MW PCL, thereby balancing out molecular entanglement to allow for snapping and simultaneously generating a stable jet by increasing the mean polymer chain length. This scalable process happens at the same high speed as regular electrospinning and therefore allows us to produce approximately 80 000 of these fragments per second per spinneret needle (Fig. S2 and Eq. S1-S3). SEM analysis (Fig. 3A) shows the results of blending 10 kDa / 80 kDa PCL at a ratio of 8:2 (Set 1) in a 30%w/v solution, displaying short fibers of  $16 \pm 7.8$  µm, whereas a ratio of 7:3 (Set 3) led to significantly longer fiber fragments of  $96.8 \pm 46.7$  µm. Comparing the fiber dimensions with 45 kDa PCL fragments (Set 2), we were able to cover a broad range of fragment sizes with well controllable aspect ratios (Fig. 3B).

Such entropy elastic effects were also described as the driving force in context of thermally-induced shape recovery of electrospun c-PCL fibers [43]. Particularly electrospun PCL fibers display pronounced chain relaxation and thus shrinkage when provided with sufficient thermal energy [44]. Although PCL displays a glass transition temperature of  $T_g \approx -60$  °C and thus at room temperature is high above glass transition, in our case, the solvent is predominantly responsible for chain mobility [45]. Consequently, the period in which the fiber is deposited and still contains enough solvent to allow for molecular relaxation is the only time in which fragmentation can take place. A previous study demonstrated that, unlike e.g. PET or PGA, PCL does not retain HFIP after electrospinning emphasizing the need of a very precise parameter set to allow for snapping [46]. We hypothesize, that the short-term presence of

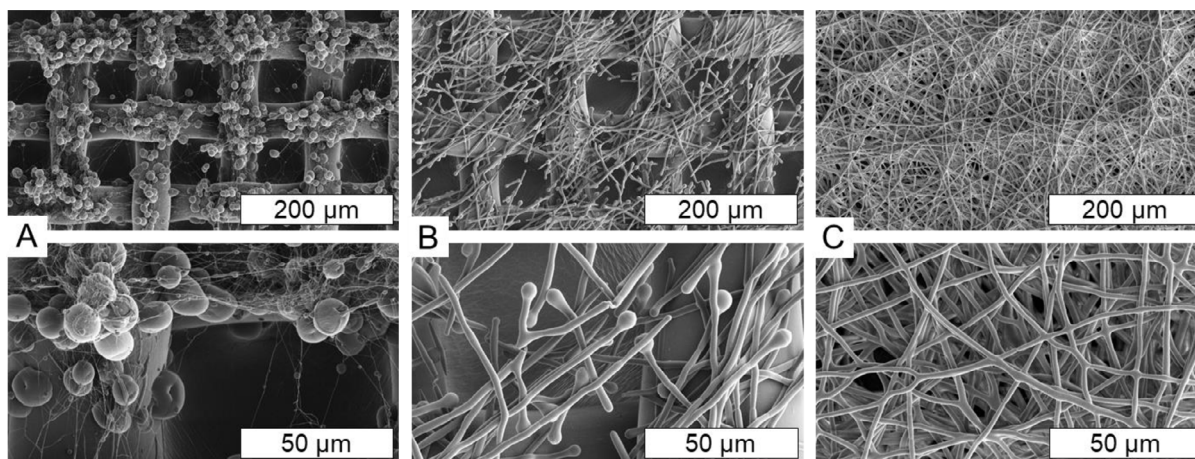


**Fig. 2.** SEM analysis of electrospun 20%w/v PCL (in HFIP) of different molecular weights (A = 10 kDa/ B = 45 kDa/ C = 80 kDa PCL) on a supporting PE mesh (mesh size 80  $\mu\text{m}$ ) as substrate. The resulting morphologies are classified as spheres (A), fragmented fibers (B) and continuous fibers (C).

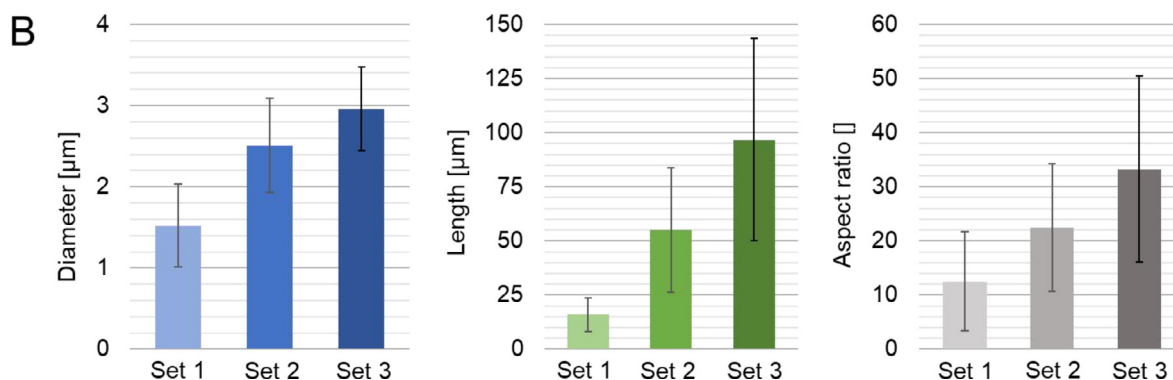
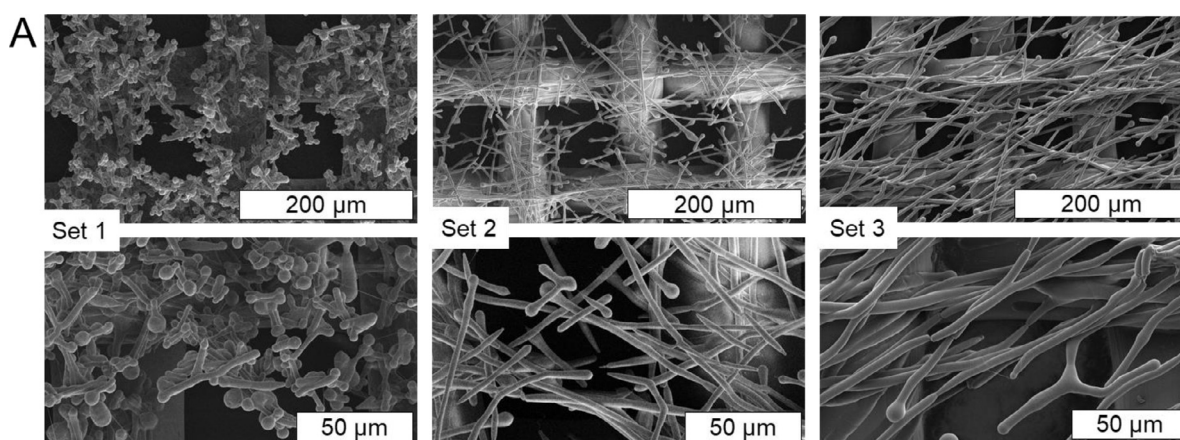


**Fig. 3.** Comparison of SEM micrographs (A) of three different sets of PCL molecular weight blends, resulting in varying degrees of fiber snapping on the substrate mesh. Set 1 and Set 3 are composed of 30%w/v PCL blends in HFIP with 8:2 (Set 1) and 7:3 (Set 3) ratio (10:80 kDa), Set 2 is 20%w/v 45 kDa PCL in HFIP. The statistical evaluation (B) of the generated morphologies is based on 100 measurements and showed an increase in diameter and length, and therefore in aspect ratio as well.

residual solvent, trapped in the fiber's core enables molecular contraction resulting in stress and fiber breaking. This is further confirmed by the fact, that low concentrations (10%w/v, 15%w/v) did not result in fiber snapping. At the breaking point, the soft core starts to creep and forms the energetically favorable conformation of a sphere. Therefore, the fiber must be provided the freedom to contract, which was given by spinning on the substrate mesh. Furthermore, contact points of the fibers on the mesh strands as well as in between the fibers prevent sliding and allow for formation of stresses leading to fiber breakage. Additional experiments,

in which the solutions were spun into an ethanol or water bath, did not result in snapping, because the fibers could evenly contract, and stress was released (data not shown).

Strikingly, although electrospinning of PCL was excessively studied within the last decades [41,47], to the best of our knowledge, nobody has ever described this morphology before. Besides the fact, that this procedure only works in a narrow parameter window, including voltage, distance, concentration, MW and solvent, this might also be attributed to the broad variety of alternative solvents that can be applied to dissolve PCL. Nevertheless, HFIP is

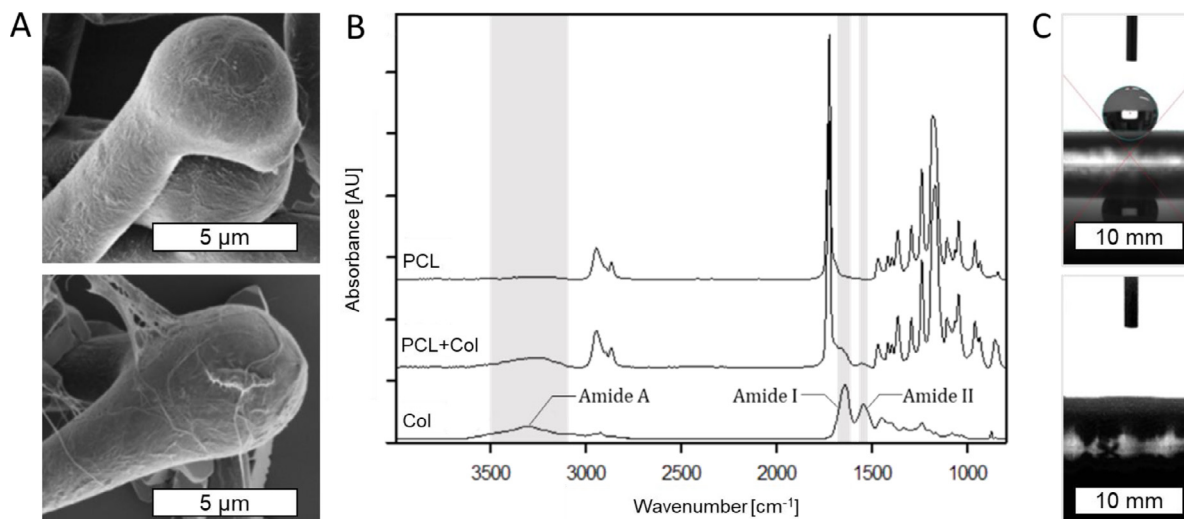


**Fig. 4.** The presence of collagen fibrils on the surface of the PCL fragments could be confirmed by SEM analysis (A). ATR-FTIR Spectra of untreated PCL, collagen coated PCL (PCL+Col) and pure collagen (Col) were recorded (B). The marked areas depict the amide A, amide I and amide II peaks that can be assigned to the presence of collagen on the surface of the coated fragments. Contact angle measurements (C) of as spun PCL fragments (top), and collagen coated (bottom) samples, where no contact angle could be measured.

known to display excellent Hansen's solubility, a parameter that was demonstrated to also play a crucial role for electrospay productivity and thus is believed to also promote the formation of the here shown dumbbell-like fiber fragments [48].

### 3.2. Surface coating of the PCL fiber fragments with collagen

Numerous studies have demonstrated the benefit of incorporating bioactive agents, that mimic ECM molecules, by blending or coating of electrospun PCL-fibers to enhance cell-performance [49,50]. To show the applicability of such strategies for our approach, PCL-fragments were aminolyzed and collagen was chemically linked to their surface in a similar way as previously published by Zhu et al. [51]. Besides the positive biological impact of collagen as a main component of the natural ECM, hydrophilization of the fiber fragments is desirable to enhance the suspendability in aqueous media – an aspect which might be highly relevant for later applications [52]. The fiber fragments were coated as described in the experimental section. Subsequently, SEM imaging was performed to exclude any interference of the chemical treatment on the dumbbell morphology. The results show that the overall structure remained intact and collagen fibrils were exposed on the surface (Fig. 4A). To further verify the presence of collagen, ATR-FTIR analysis was performed referring to pure PCL and pure collagen samples (Fig. 4B) showing the chemical modification via detectable surface groups. The characteristic bands for PCL at the positions 2945 cm<sup>-1</sup> and 2866 cm<sup>-1</sup> for CH<sub>2</sub> stretching, at 1720 cm<sup>-1</sup> (stretching of carbonyl groups), at 1295 cm<sup>-1</sup> (C–O stretching) and the C–O–C stretching at 1240 cm<sup>-1</sup> and 1168 cm<sup>-1</sup> can be detected also in the coated sample (PCL+Col) displaying molecular integrity of PCL also after chemical treatment [50,53–56]. With the collagen-coating (PCL+Col), additional peaks could be detected at 3299 cm<sup>-1</sup>, 1647 cm<sup>-1</sup> and 1534 cm<sup>-1</sup>, which are assigned to the Amide A, Amide I and Amide II bands of collagen (Fig. 4B–Col), confirming successful coating [57]. Additional analysis applying XPS detected 5.9% nitrogen groups on the surface of the PCL fragments after the coating procedure (0% nitrogen in uncoated state), indicating that the chemical crosslinking was successful as further confirmed via EDX (Fig. S5 and S6).

Contact angle measurements showed a significant decrease in hydrophobicity of the PCL fragments by the coating procedure

(Fig. 4C). The detected reference contact angle for the sample supporting glass substrate was  $27.6 \pm 3.3^\circ$  whereas untreated PCL fiber mats resulted in a contact angle of  $129 \pm 1.0^\circ$ . The contact angle on collagen-coated fragments could not be determined due to instant wetting of the samples.

Summarizing these results, we could clearly demonstrate the applicability of chemically coating PCL-dumbbells with collagen to further assess their performance as a substrate for in-vitro cell-culture.

### 3.3. Cell culture experiments

To test, whether PCL-fiber fragmentation affects the interaction of cells with the collagen-coated PCL-fiber fragments of different morphologies, we morphologically assessed U87 glioblastoma cells using scanning electron microscopy (SEM). This revealed that cells cultured on non-aligned continuous fiber constructs, even though they were colonizing the surface, showed limited cell spreading and tended to grow in clusters (Fig. 5A). Similarly, cells cultured on aligned, continuous fiber constructs were not fully spread and primarily grew in clusters (Fig. 5B), even though they showed an alignment parallel to the PCL-fiber orientation. In contrast, cells cultured on mixed morphologies consisting of aligned continuous fibers and aligned fragments were well spread and homogeneously covered the surface (Fig. 5C), suggesting that the presence of fragmented fibers improved the cell-collagen-fiber interaction. In line with this, cells cultured exclusively on fragmented fibers showed the best spreading behavior and most even surface coverage (Fig. 5D). These data demonstrate that PCL-fiber fragmentation can considerably improve the interaction of cells by mimicking ECM contact possibilities with the fiber surface via the cell adhesion through integrin-collagen interaction. Additional live cell imaging experiments over the course of 3 days showed a high affinity of U87 cells towards fiber fragments, actively adhering to them, carrying them around and even forming clusters (Fig. S4, movie files S8 and S9). Complementary live-dead assays (Figure S3) displayed high cell viability of 98–99% after 24 h of cultivation time, irrespective if seeded on the positive control of a collagen coated cell culture plate or on collagen coated PCL-fibers.

To investigate changes in cell morphology initiated by binding of integrins following fiber induced changes in cell-morphology or

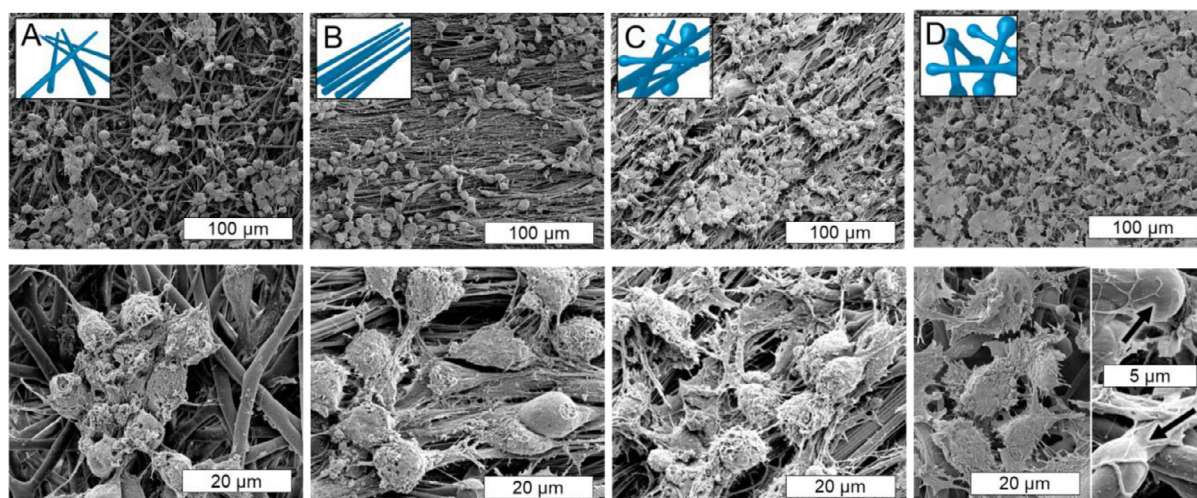


**Fig. 5.** SEM analysis of U87 glioblastoma cells after 96 h cultivation on different morphologies of collagen-coated electrospun PCL substrates. The investigated morphologies are random continuous fibers (A), aligned continuous fibers (B), mixed morphology with aligned, continuous fibers and fragments (C) and non-oriented dumbbell shaped fragments (D).

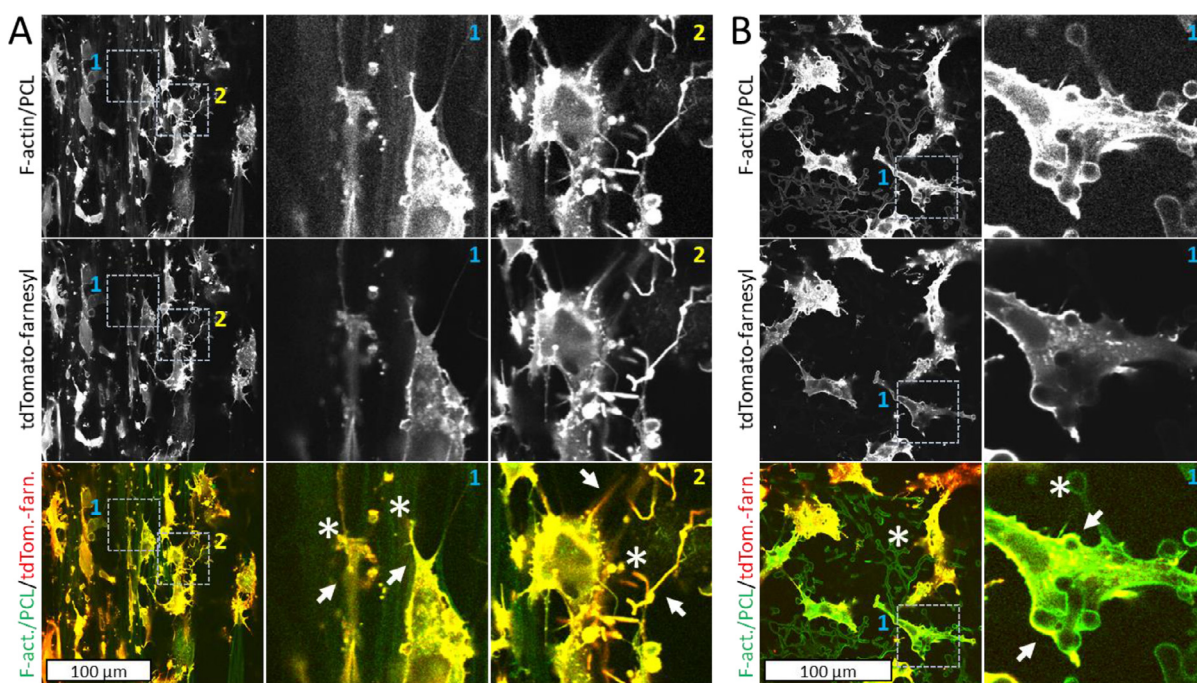


**Fig. 6.** PCL-fiber fragmentation promotes cell adhesion and spreading. (A) Confocal micrographs showing F-actin staining with PCL-autofluorescence (upper panel, lower panel asterisks) and tdTomato-farnesyl staining (middle panel) of U87 morphology reporter cells on constructs with mixed, aligned PCL-fiber morphology. Note elongated morphology of cells in regions of fragmented fiber morphology (insert 1, asterisks) with robust protrusions extending along the fibers (insert 1, arrows), as opposed to round cell morphology in regions of continuous fiber morphology (insert 2, asterisk) with multiple, filopodia-like protrusions (insert 2, arrows). (B) Confocal micrographs showing F-actin staining with PCL-autofluorescence (upper panel; lower panel asterisk) and tdTomato-farnesyl staining (middle panel) of U87 morphology reporter cells on constructs with non-aligned, fragmented PCL-fiber morphology. Note well spread cell morphology and multiple interactions of cells with the rounded ends of dumbbell-shaped fiber fragments (insert 1, arrows), characterized by abundant plasma-membrane and F-actin staining.

cell migration, we used immunocytochemical staining of F-actin, following confocal microscopy. With this approach, sample preparation does not involve harsh drying procedures. Integrin-mediated cell adhesion often results in cell spreading and the formation of focal adhesions. To deepen the morphological assessment of these cells, we generated lentivirally transduced U87 reporter cells. These cells stably express tdTomato red-fluorescent protein carrying a membrane-localizing farnesylation-signal, resulting in a red fluorescence of the cell membrane. Reporter cells were cultured on mixed PCL-fiber morphologies and on fragmented fiber constructs, followed by fixation and Alexa488-phalloidin labeling of

the actin cytoskeleton. F-actin staining determines the morphology of adherent cells and is controlled by integrin adhesion receptors activated by contact to collagen coated-fibers. Analyzing F-actin in combination with the red-fluorescent membrane gives us the possibility to study different cell morphologies due to lesser or higher contact options to collagen leading to more contact points and with that different cell morphologies. In reporter cell cultures on mixed fiber-morphologies, those cells in regions with fragmented fibers, as assessed by PCL-autofluorescence (Fig. 6A insert 1, asterisks), showed an elongated cell morphology with robust, F-actin-containing protrusions extending along the PCL-fibers

(Fig. 6A insert 1, arrows), indicating that the cells adhered well to fragmented PCL-fibers. In contrast, cells in regions with continuous fibers (Fig. 6A insert 2, asterisk) were more rounded and displayed multiple, small, filopodial protrusions, indicative of an impaired cell-collagen-fiber adhesion (Fig. 6A insert 2, arrows). Consistent with our SEM-data, we observed that reporter cells cultured exclusively on fragmented fibers (Fig. 6B asterisks) showed the most extensive spreading, possibly due to more pronounced contacts between collagen and cell-integrins. Importantly, cells often showed multiple interactions with the rounded ends of PCL-fiber fragments, that were associated with high F-actin fluorescence intensity (Fig. 6B insert, arrows).

These findings suggest that the rounded ends of the dumbbell-shape provide a particularly efficient environment for integrin-based cell adhesions to the collagen-fibers. It is possible that their increased diameter leads to the best and maximal possible cell-integrin to collagen-dumbbell contacts. Our findings are in line with previous reports demonstrating that substrate curvature has critical effects on cell adhesive processes [58,59]. Gingras and Ginsberg (2020) demonstrated that physical deformation of the plasmamembrane can result in integrin activation [60]. Consistent with this, Li et al. (2017) reported that substrate curvature in the low micrometer range controlled integrin activation, proliferative and cytoskeletal signaling, and angiogenic differentiation of human adipose derived stem cells [61]. Similarly, Ozdemir et al. (2013) showed that RhoA-GTPase activation, actomyosin contraction, cell stiffening and osteogenic differentiation of osteoprogenitor cells on PMMA-substrates was increased on electrospun PMMA-fibers of low micrometer range diameter compared to flat surface substrates [62]. Hence, controlled fragmentation of PCL-fibers resulting in dumbbell-shaped fragments with defined lengths and rounded ends of tunable diameter may provide a possibility to efficiently harness substrate curvature effects for tailoring the cell adhesive properties of PCL-based tissue engineering constructs.

#### 4. Conclusion

In this work, we could for the first time demonstrate and control the formation of dumbbell-like PCL-structures produced by a simple electrospinning setup with a precisely balanced parameter set. Entropy-elasticity combined with the process-induced anisotropic molecular arrangement is hypothesized to be the driving force behind fiber snapping. Based on these findings, MW of PCL was identified to be crucial for the formation of such morphologies and could be applied to control the aspect ratio of fiber fragments. Considering the fact, that such morphologies might be appealing for cells as they display attractive micro-meter-range dimensions, in-vitro testing with U87 glioblastoma cells was performed. To render the surface biofunctional, collagen coating was applied, moreover leading to hydrophilization and thus improved suspendability of the fragments in water. Strikingly, it was shown that particularly the round-shaped ends of dumbbell-like fragments provide highly efficient structures for integrin-based cell adhesion. Although FDA-approved PCL is one of the most widely used biopolymers in the biomedical field and electrospinning is a popular method to process it into fibers, to the best of our knowledge, this is the first time such micro-dumbbells were systematically documented. Considering, that dumbbell-like structures combine morphological features of spheres and fibers, this new class of polymeric particles will be further explored as e.g. anisotropic filler material in biofabrication and cosmetics as well as in the field of injectables and drug delivery systems.

#### Author statement

David Sonnleitner: Roles/Writing – original draft, Formal analysis, Investigation, Methodology, Visualization

Natascha Schäfer: Data curation; Formal analysis, Methodology, Visualization, Investigation, Writing – review & editing

Annalena Wieland: Investigation, Visualization

Lena Fischer: Investigation

Patrick Pasberg: Investigation

Ingo Thievensen: Formal analysis, Methodology, Visualization, Investigation, Writing – review & editing, Resources

Gregor Lang: Conceptualization, Project administration, Data curation, Funding acquisition, Resources, Methodology, Supervision, Validation, Resources, Writing – review & editing

#### Data availability statement

The manuscript includes all data that are required to reproduce these findings. For raw data (such as FT-IR measurements, SEM-imaging, cell-culture imaging) please contact the corresponding author.

#### Declaration of Competing Interest

None.

#### Acknowledgements

This work has been funded by the German Research Foundation (DFG, [Deutsche Forschungsgemeinschaft](#)) – project number [326998133](#), SFB/TRR 225 “Biofabrication” (subprojects A07, PI: Gregor Lang and B06, PI: Ingo Thievensen). Natascha Schaefer was supported by funds of the Bavarian State Ministry of Science and the Arts and the University of Würzburg to the Graduate School of Life Sciences (GSLs), University of Würzburg. Dana Wegmann is greatly acknowledged for her excellent assistance in cell culture experiments. We thank Dr. Ulrich Mansfeld and Morten Weiß for kindly supporting us with EDX and XPS analysis.

#### Supplementary materials

Supplementary material associated with this article can be found, in the online version, at doi:[10.1016/j.apmt.2021.101097](#).

#### References

- [1] S. Kumbar, C. Laurencin, M. Deng, *Natural and Synthetic Biomedical Polymers*, Elsevier, Burlington, Massachusetts, San Diego, California, 2014.
- [2] F.J. van Natta, J.W. Hill, W.H. Carothers, Studies of polymerization and ring formation. XXIII. 1  $\epsilon$ -caprolactone and its polymers, *J. Am. Chem. Soc.* 56 (1934) 455–457, doi:[10.1021/ja01317a053](#).
- [3] R.M. Ginde, R.K. Gupta, In vitro chemical degradation of poly(glycolic acid) pellets and fibers, *J. Appl. Polym. Sci.* 33 (1987) 2411–2429, doi:[10.1002/app.1987.070330712](#).
- [4] M.A. Woodruff, D.W. Hutmacher, The return of a forgotten polymer—polycaprolactone in the 21st century, *Prog. Polym. Sci.* 35 (2010) 1217–1256, doi:[10.1016/j.progpolymsci.2010.04.002](#).
- [5] R.S. Bezwada, D.D. Jamiolkowski, I.Y.Y. Lee, V. Agarwal, S. Trenka-Benthin, M. Ernetta, J. Suryadevara, A. Yang, S. Liu, Monocryl suture, a new ultrapliable absorbable monofilament suture, *Biomaterials* 16 (15) (1995) 1141–1148, doi:[10.1016/0142-9612\(95\)93577-z](#).
- [6] G. Ma, C. Song, H. Sun, J. Yang, X. Leng, A biodegradable levonorgestrel-releasing implant made of PCL/F68 compound as tested in rats and dogs, *Contraception* 74 (2006) 141–147, doi:[10.1016/j.contraception.2006.02.013](#).
- [7] K.W. Ng, H.N. Achuth, S. Mochhala, T.C. Lim, D.W. Hutmacher, In vivo evaluation of an ultra-thin polycaprolactone film as a wound dressing, *J. Biomater. Sci. Polym. Ed.* 18 (2007) 925–938, doi:[10.1163/156856207781367693](#).
- [8] A. Nilsson, M. Wiig, H. Alnehill, M. Berggren, S. Björnum, M. Geijer, P. Kopylov, C. Sollerman, The Artelon CMC spacer compared with tendon interposition arthroplasty, *Acta Orthop.* 81 (2010) 237–244, doi:[10.3109/17453671003635835](#).

- [9] K.-H. Schuckert, S. Jopp, S.-H. Teoh, Mandibular defect reconstruction using three-dimensional polycaprolactone scaffold in combination with platelet-rich plasma and recombinant human bone morphogenetic protein-2: de novo synthesis of bone in a single case, *Tissue Eng. Part A* 15 (2009) 493–499, doi:10.1089/ten.tea.2008.0033.
- [10] M.P. Arrieta, A.L. Gil, M. Yusef, J.M. Kenny, L. Peponi, Electrospinning of PCL-based blends: processing optimization for their scalable production, *Materials* (2020) 13.
- [11] A.N. Boyandin, L.M. Dvoinina, A.G. Sukovaty, A.A. Sukhanova, Production of porous films based on biodegradable polyesters by the casting solution technique using a co-soluble porogen (Camphor), *Polymers (Basel)* (2020) 12, doi:10.3390/polym12091950.
- [12] S.Y. Kim, J.-Y. Hwang, U.S. Shin, Preparation of nano/macroporous polycaprolactone microspheres for an injectable cell delivery system using room temperature ionic liquid and camphene, *J. Colloid Interface Sci.* 465 (2016) 18–25, doi:10.1016/j.jcis.2015.11.055.
- [13] Z. Meng, J. He, Z. Cai, F. Wang, J. Zhang, L. Wang, R. Ling, D. Li, Design and additive manufacturing of flexible polycaprolactone scaffolds with highly-tunable mechanical properties for soft tissue engineering, *Mater. Des.* 189 (2020) 108508, doi:10.1016/j.matdes.2020.108508.
- [14] E. Nyberg, A. Rindone, A. Dorafshar, W.L. Grayson, Comparison of 3D-printed poly- $\epsilon$ -caprolactone scaffolds functionalized with tricalcium phosphate, hydroxyapatite, bio-oss, or decellularized bone matrix-sup, *Tissue Eng. Part A* 23 (2017) 503–514, doi:10.1089/ten.tea.2016.0418.
- [15] F. Zhang, T. Zhou, Y. Liu, J. Leng, Microwave synthesis and actuation of shape memory polycaprolactone foams with high speed, *Sci. Rep.* 5 (2015) 11152, doi:10.1038/srep11152.
- [16] J. Doshi, D.H. Reneker, Electrospinning process and applications of electrospun fibers, *J. Electrostat.* 35 (1995) 151–160, doi:10.1016/0304-3886(95)00041-8.
- [17] A. Greiner, J.H. Wendorff, Electrospinning: a fascinating method for the preparation of ultrathin fibers, *Angew. Chem. Int. Ed. Engl.* 46 (2007) 5670–5703, doi:10.1002/anie.200604646.
- [18] Y.M. Shin, M.M. Hohman, M.P. Brenner, G.C. Rutledge, Experimental characterization of electrospinning: the electrically forced jet and instabilities, *Polymer* 42 (2001) 9955–9967, doi:10.1016/S0032-3861(01)00540-7.
- [19] A.L. Yarin, S. Koombhongse, D.H. Reneker, Bending instability in electrospinning of nanofibers, *J. Appl. Phys.* 89 (2001) 3018–3026, doi:10.1063/1.1333035.
- [20] S. Agarwal, J.H. Wendorff, A. Greiner, Progress in the field of electrospinning for tissue engineering applications, *Adv. Mater.* (Deerfield Beach, Fla.) 21 (2009) 3343–3351, https://doi.org/10.1002/adma.200803092.
- [21] M. Bognitzki, W. Czado, T. Frese, A. Schaper, M. Hellwig, M. Steinhart, A. Greiner, J.H. Wendorff, Nanostructured fibers via electrospinning, *Adv. Mater.* 13 (2001) 70–72, doi:10.1002/1521-4095(200101)13:1<70:AID-ADMA70>3.0.CO;2-H.
- [22] R. Vasita, D.S. Katti, Nanofibers and their applications in tissue engineering, *Int. J. Nanomed.* 1 (2006) 15–30, doi:10.2147/nano.2006.1.1.15.
- [23] C. Frantz, K.M. Stewart, V.M. Weaver, The extracellular matrix at a glance, *J. Cell. Sci.* 123 (2010) 4195–4200, doi:10.1242/jcs.023820.
- [24] B. Alberts, *Molecular Biology of the Cell*, 5th Ed., Garland Science, New York, 2008.
- [25] D.S. Harburger, D.A. Calderwood, Integrin signalling at a glance, *J. Cell. Sci.* 122 (2009) 159–163, doi:10.1242/jcs.018093.
- [26] S. Schmidt, P. Friedl, Interstitial cell migration: integrin-dependent and alternative adhesion mechanisms, *Cell Tissue Res.* 339 (2010) 83–92, doi:10.1007/s00441-009-0892-9.
- [27] S. Wiesner, K.R. Legate, R. Fässler, Integrin-actin interactions, *Cell. Mol. Life Sci. CMLS* 62 (2005) 1081–1099, doi:10.1007/s00018-005-4522-8.
- [28] J.K. Wise, A.L. Yarin, C.M. Megaridis, M. Cho, Chondrogenic differentiation of human mesenchymal stem cells on oriented nanofibrous scaffolds: engineering the superficial zone of articular cartilage, *Tissue Eng. Part A* 15 (2009) 913–921, doi:10.1089/ten.tea.2008.0109.
- [29] A. Balguid, A. Mol, M.H. van Marion, R.A. Bank, C.V.C. Bouten, F.P.T. Baaijens, Tailoring fiber diameter in electrospun poly( $\epsilon$ -caprolactone) scaffolds for optimal cellular infiltration in cardiovascular tissue engineering, *Tissue Eng. Part A* 15 (2009) 437–444, doi:10.1089/ten.tea.2007.0294.
- [30] E. Schnell, K. Klinkhammer, S. Balzer, G. Brook, D. Klee, P. Dalton, J. Mey, Guidance of glial cell migration and axonal growth on electrospun nanofibers of poly- $\epsilon$ -caprolactone and a collagen/poly- $\epsilon$ -caprolactone blend, *Biomaterials* 28 (2007) 3012–3025, doi:10.1016/j.biomaterials.2007.03.009.
- [31] N. Krithica, V. Natarajan, B. Madhan, P.K. Sehgal, A.B. Mandal, Type I collagen immobilized poly(caprolactone) nanofibers: characterization of surface modification and growth of fibroblasts, *Adv. Eng. Mater.* 14 (2012) B149–B154, doi:10.1002/adem.201180035.
- [32] C. Licht, J.C. Rose, A.O. Anarkoli, D. Blondel, M. Roccio, T. Haraszti, D.B. Gehlen, J.A. Hubbell, M.P. Lutolf, L. de Laporte, Synthetic 3D PEG-anisogel tailored with fibronectin fragments induce aligned nerve extension, *Biomacromolecules* 20 (2019) 4075–4087, https://doi.org/10.1021/acs.biomac.9b00891.
- [33] H. Li, H. Wan, T. Xia, M. Chen, Y. Zhang, X. Luo, X. Li, Therapeutic angiogenesis in ischemic muscles after local injection of fragmented fibers with loaded traditional Chinese medicine, *Nanoscale* 7 (2015) 13075–13087, doi:10.1039/C5NR02005K.
- [34] W. Chen, Y. Xu, Y. Li, L. Jia, X. Mo, G. Jiang, G. Zhou, 3D printing electrospinning fiber-reinforced decellularized extracellular matrix for cartilage regeneration, *Chem. Eng. J.* 382 (2020) 122986, doi:10.1016/j.cej.2019.122986.
- [35] F.-L. Zhou, P.L. Hubbard Cristinacce, S.J. Eichhorn, G.J.M. Parker, Preparation and characterization of polycaprolactone microspheres by electrospinning, *Aerosol. Sci. Tech.* 50 (2016) 1201–1215, doi:10.1080/02786826.2016.1234707.
- [36] I.K. Kwon, S. Kidoaki, T. Matsuda, Electrospun nano- to microfiber fabrics made of biodegradable copolyesters: structural characteristics, mechanical properties and cell adhesion potential, *Biomaterials* 26 (2005) 3929–3939, doi:10.1016/j.biomaterials.2004.10.007.
- [37] A.O. Lobo, S. Afewerki, M.M.M. de Paula, P. Ghannadian, F.R. Marciano, Y.S. Zhang, T.J. Webster, A. Khademhosseini, Electrospun nanofiber blend with improved mechanical and biological performance, *Int. J. Nanomed.* 13 (2018) 7891–7903, doi:10.2147/IJN.S175619.
- [38] I.Y. Enis, J. Vojtech, T.G. Sadikoglu, Alternative solvent systems for polycaprolactone nanowebs via electrospinning, *J. Ind. Textiles* 47 (2017) 57–70, doi:10.1177/15280837166634032.
- [39] J. Schindelin, I. Arganda-Carreras, E. Frise, V. Kaynig, M. Longair, T. Pietzsch, S. Preibisch, C. Rueden, S. Saalfeld, B. Schmid, J.-Y. Tinevez, D.J. White, V. Hartenstein, K. Eliceiri, P. Tomancak, A. Cardona, Fiji: an open-source platform for biological-image analysis, *Nat. Methods* 9 (2012) 676–682, doi:10.1038/nmeth.2019.
- [40] E.K. Kostakova, L. Meszaros, G. Maskova, L. Blazkova, T. Turcsan, D. Lukas, Crystallinity of electrospun and centrifugal spun polycaprolactone fibers: a comparative study, *J. Nanomater.* (2017) 2017.
- [41] A. Cipitria, A. Skelton, T.R. Dargaville, P.D. Dalton, D.W. Huttmacher, Design, fabrication and characterization of PCL electrospun scaffolds—a review, *J. Mater. Chem.* 21 (2011) 9419–9453.
- [42] F.L. Zhou, P.L.H. Cristinacce, S.J. Eichhorn, G.J.M. Parker, Preparation and characterization of polycaprolactone microspheres by electrospinning, *Aerosol. Sci. Tech.* 50 (2016) 1201–1215.
- [43] T. Gong, W.B. Li, H.M. Chen, L. Wang, S.J. Shao, S.B. Zhou, Remotely actuated shape memory effect of electrospun composite nanofibers, *Acta Biomater.* 8 (2012) 1248–1259.
- [44] Y. Gao, K. Sim, X. Yan, J. Jiang, J.W. Xie, C.J. Yu, Thermally triggered mechanically destructive electronics based on electrospun poly( $\epsilon$ -caprolactone) nanofibrous polymer films, *Sci. Rep.-Uk* 7 (2017), https://doi.org/10.1038/s41598-017-01026-6.
- [45] T.P. Gumedde, A.S. Luyt, M.K. Hassan, R.A. Perez-Camargo, A. Tercjak, A.J. Muller, Morphology, nucleation, and isothermal crystallization kinetics of poly( $\epsilon$ -caprolactone) mixed with a polycarbonate/MWCNTs masterbatch, *Polym.-Basel* 9 (2017).
- [46] A.R. D'Amato, M.T.K. Bramson, D.L. Puhl, J. Johnson, D.T. Corr, R.J. Gilbert, Solvent retention in electrospun fibers affects scaffold mechanical properties, *Electrospinning* 2 (2018) 15–28, doi:10.1515/esp-2018-0002.
- [47] M.J. Mochane, T.S. Motosoeneng, E.R. Sadiku, T.C. Mokhena, J.S. Sefadi, Morphology and properties of electrospun PCL and its composites for medical applications: a mini review, *Appl. Sci.-Basel* 9 (2019).
- [48] S.C. Zhang, C. Campagne, F. Salaun, Influence of Solvent Selection in the Electrospinning Process of Polycaprolactone, *Appl. Sci.-Basel* 9 (2019).
- [49] C. Eriskin, D.M. Kalyon, H. Wang, Functionally graded electrospun polycaprolactone and beta-tricalcium phosphate nanocomposites for tissue engineering applications, *Biomaterials* 29 (2008) 4065–4073, doi:10.1016/j.biomaterials.2008.06.022.
- [50] J. Chutipakdeevong, U. Ruktanonchai, P. Supaphol, Hybrid biomimetic electrospun fibrous mats derived from poly( $\epsilon$ -caprolactone) and silk fibroin protein for wound dressing application, *J. Appl. Polym. Sci.* (2014) n/a-n/a, doi:10.1002/app.41653.
- [51] Y. Zhu, C. Gao, X. Liu, J. Shen, Surface modification of polycaprolactone membrane via aminolysis and biomacromolecule immobilization for promoting cytocompatibility of human endothelial cells, *Biomacromolecules* 3 (2002) 1312–1319, doi:10.1021/bm020074y.
- [52] D. Gupta, J. Venugopal, M.P. Prabhakaran, V.R.G. Dev, S. Low, A.T. Choon, S. Ramakrishna, Aligned and random nanofibrous substrate for the in vitro culture of Schwann cells for neural tissue engineering, *Acta Biomater.* 5 (2009) 2560–2569, doi:10.1016/j.actbio.2009.01.039.
- [53] L. Liverani, M.S. Killian, A.R. Boccaccini, Fibronectin Functionalized Electrospun Fibers by Using Benign Solvents: best Way to Achieve Effective Functionalization, *Front. Bioeng. Biotechnol.* 7 (2019) 68, doi:10.3389/fbioe.2019.00068.
- [54] L. Ghasemi-Mobarakeh, M.P. Prabhakaran, M. Morshed, M.-H. Nasr-Esfahani, S. Ramakrishna, Electrospun poly( $\epsilon$ -caprolactone)/gelatin nanofibrous scaffolds for nerve tissue engineering, *Biomaterials* 29 (2008) 4532–4539, doi:10.1016/j.biomaterials.2008.08.007.
- [55] A.K. Gaharwar, M. Nikkhah, S. Sant, A. Khademhosseini, Anisotropic poly(glycerol sebacate)-poly( $\epsilon$ -caprolactone) electrospun fibers promote endothelial cell guidance, *Biofabrication* 7 (2014) 15001, doi:10.1088/1758-5090/7/1/015001.
- [56] S.A. Catledge, W.C. Clem, N. Shrikishen, S. Chowdhury, A.V. Stanishevsky, M. Koopman, Y.K. Vohra, An electrospun triphasic nanofibrous scaffold for bone tissue engineering, *Biomed. Mater.* 2 (2007) 142–150, doi:10.1088/1748-6041/2/2/013.
- [57] T. Riaz, R. Zeeshan, F. Zarif, K. Ilyas, N. Muhammad, S.Z. Safi, A. Rahim, S.A.A. Rizvi, I.U. Rehman, FTIR analysis of natural and synthetic collagen, *Appl. Spectrosc. Rev.* 53 (2018) 703–746, doi:10.1080/05704928.2018.1426595.
- [58] T. Yamashita, P. Kollmannsberger, K. Mawatari, T. Kitamori, V. Vogel, Cell sheet mechanics: how geometrical constraints induce the detachment of cell sheets from concave surfaces, *Acta Biomater.* 45 (2016) 85–97, doi:10.1016/j.actbio.2016.08.044.

- [59] M.-C. Kim, C. Kim, L. Wood, D. Neal, R.D. Kamm, H.H. Asada, Integrating focal adhesion dynamics, cytoskeleton remodeling, and actin motor activity for predicting cell migration on 3D curved surfaces of the extracellular matrix, *Integr. Biol. Quant. Biosci. Nano Macro* 4 (2012) 1386–1397, doi:[10.1039/c2ib20159c](https://doi.org/10.1039/c2ib20159c).
- [60] A.R. Gingras, M.H. Ginsberg, Signal transduction: physical deformation of the membrane activates integrins, *Curr. Biol. CB* 30 (2020) R397–R400, doi:[10.1016/j.cub.2020.02.068](https://doi.org/10.1016/j.cub.2020.02.068).
- [61] Z. Li, W. Wang, X. Xu, K. Kratz, J. Zou, L. Lysyakova, M. Heuchel, A. Kurtz, M. Gossen, N. Ma, A. Lendlein, Integrin  $\beta$ 1 activation by micro-scale curvature promotes pro-angiogenic secretion of human mesenchymal stem cells, *J. Mater. Chem. B* 5 (2017) 7415–7425, doi:[10.1039/c7tb01232b](https://doi.org/10.1039/c7tb01232b).
- [62] T. Ozdemir, L.-C. Xu, C. Siedlecki, J.L. Brown, Substrate curvature sensing through Myosin IIa upregulates early osteogenesis, *Integr. Biol. Quant. Biosci. Nano Macro* 5 (2013) 1407–1416, doi:[10.1039/c3ib40068a](https://doi.org/10.1039/c3ib40068a).